Nonlinear spontaneous symmetry breaking in active polar films

Dario Cortese, Jens Eggers and Tanniemola B. Liverpool

School of Mathematics, University of Bristol - Bristol BS8 1TW, UK

Abstract – The behaviour of an active polar suspension in a fluid film is analysed in the vanishing Reynolds number limit. We perform a detailed study of the transitions to spontaneously flowing steady states and their associated density variations. Beyond the onset of instability, we find a new transverse symmetry breaking of the flow generated in the film. This spontaneous symmetry breaking is observed despite symmetric boundary conditions (with respect to orientation) on either side of the film. We study this new phenomenon by means of numerical simulations and nonlinear theory, showing that it can be ascribed to the *nonlinear* coupling, characteristic of polar active systems, of the density gradients with the flow velocity and the orientation field. As such a theoretical analysis based on linear stability arguments typically used to identify phase boundaries is unable to describe it. An extension of the theory to allow for higher-density regimes is also proposed.

Introduction. – Active materials [1] are a class of soft materials maintained out of equilibrium by internal energy sources, generally a suspension of active units. Examples of such materials can be found in biological contexts: bacterial colonies [2–5], cytoskeletal filaments and motor proteins [6,7], and the cell cytoskeleton [8–10] are only some of them. Non-biological systems [11,12], for example a layer of vibrated granular rods [13,14], also show similar behaviour. The key property that distinguishes active matter from more familiar non-equilibrium systems, such as fluids under shear, is that the energy input that maintains the system out of equilibrium comes from each constituent, rather than the boundaries. Each active unit goes through a cycle during which it dissipates energy and fuels internal changes, thus leading to motion.

Typically, active systems consist of suspensions in a fluid of anisotropic self-propelled particles of two types: polar ones, with a head and a tail, and apolar ones that are head-tail symmetric [1] and are often called *active liquid crystals*. Hence they are characterised by condensed phases typical of liquid crystals [15], along with a range of new phenomena. Apolar particles can form phases with nematic order, characterized by a macroscopic axis of mean orientation identified by a unit vector **n** and global symmetry for **n** → −**n**. Polar particles can order in both nematic and polar phases. The polar phase is again characterized by a mean orientation axis **P**, but **P** ≠ −**P**.

One of the most remarkable properties of confined active liquid crystals is the dynamical emergence of spontaneously flowing states (both stationary and oscillatory) starting from a uniform aligned homogeneous state [16–18]. These occur because local orientational order generates active stresses, and these are in turn balanced by the fluid flow. This leads to states that can support local inhomogeneities in the velocity of the fluid and the local alignment of the particles, while maintaining a net zero force. Thus, active liquid crystal films, beyond a critical film thickness or activity can generate motion even in the absence of externally applied forces [17], in contrast to their passive counterparts [15]. The transition from stationary to flowing states and resulting non-equilibrium phase diagrams are usually obtained via linear stability analyses [16,17,19–22].

Active polar fluids have a rich spectrum of behaviours [19–22]. Indeed, like active nematics [17], they exhibit steady spontaneous flow. Unlike active nematics, however, where the particle concentration remains practically uniform in the spontaneously flowing state [17], spontaneous flow in polar fluids is accompanied by "concentration banding" [20], *i.e.*, a sharp gradient in the concentration of particles across the film. This is due to couplings of concentration gradients to the polar director, which are not allowed for systems with nematic symmetry [15].
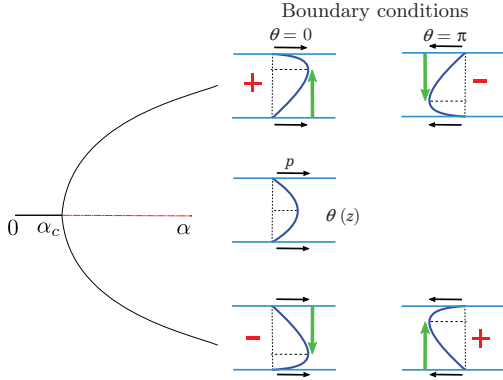
Fig. 1: (Colour online) Symmetry breaking in an active polar film: as the activity is increased, the orientation profile $\theta(z)$ becomes unstable and a bifurcation with two asymmetric states occurs. A small asymmetry in the initial conditions (ICs) determines the final state. For the same ICs, a flip in the BCs selects a different state.

In this letter we show that active polar films present an even richer behaviour due to the *nonlinearity* of the dynamics. The coupling terms that dominate the dynamics beyond the onset of spontaneous flow are nonlinear and induce an *additional* spontaneous symmetry breaking in the variations of the orientation and density fields. Here we study an infinite thin planar active fluid film with free boundary surfaces on both sides. Previous work on the same system [20] with asymmetric boundary conditions (BCs) has provided a phase diagram using a combination of numerical calculations and linear stability analysis. In this letter, we analyse for the first time the case of *symmetric* BCs, and show that a *spontaneous*, *discrete* symmetry breaking is exhibited by the system in the direction of the film thickness (*i.e.* orthogonal to the spontaneous flow direction), with higher concentration gradients and orientation alignment on one side of the film compared to the other. The initial conditions select between the two equivalent states shown in fig. 1, one where the maximum orientation lies in the lower half of the film, and the other with the same profile but with maximum in the upper half. Interestingly, *for the same initial condition*, the sign of the broken symmetry in the eventual steady-state can be changed by a symmetric flip of the *boundary conditions* at the edges of the film (thus in a direction parallel to the flow). This phenomenon, which cannot be described by a linear analysis of the first unstable modes, is identified and described by means of a nonlinear stability analysis and confirmed by numerical simulations.

Geometry and governing equations. – Our model of a polar active suspension (see fig. 2) consists of an infinite two-dimensional fluid film, confined between two free surfaces at $z = 0$ and $z = L$, in which a suspension of anisotropic particles of length $\ell \ll L$ is immersed.

We consider polar self-propelling particles with constant speed and focus on spatial variations of the orientation
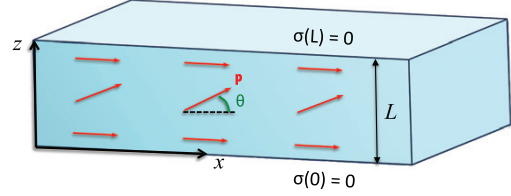
Fig. 2: (Colour online) Schematic representation of the active fluid film of thickness L. The polar rods form an angle θ with respect to the direction x.

of the polarization vector $\mathbf{P}$. The total density of the suspension is $\rho = Mc + \rho_f$, with ρ_f the fluid density, c is the concentration of active particles and their mass M is assumed to be constant. Therefore, we have $\rho_f = \text{const}$ and $\nabla \cdot \mathbf{u} = 0$, with $\mathbf{u}$ being the flow velocity field.

The dynamical equations for an active suspension are now well accepted [1] with a generic structure that can be applied to a broad class of active liquid crystals. Some terms in the equations, which are present at equilibrium, can be obtained from a non-equilibrium analogue of a free energy while others are due to the intrinsically non-equilibrium nature of these systems. The non-equilibrium free energy F is given by [1]

$$F = \int_{\mathbf{r}} \left\{ \frac{K_1}{2} (\nabla \cdot \mathbf{P})^2 + \frac{K_3}{2} (\nabla \times \mathbf{P})^2 + B_1 \frac{c - c_0}{c_0} \nabla \cdot \mathbf{P} \right.$$
$$+ \frac{B_2}{2} |\mathbf{P}|^2 \nabla \cdot \mathbf{P} + \frac{B_3}{3c_0} |\mathbf{P}|^2 \mathbf{P} \cdot \nabla c$$
$$\left. + \frac{C}{2} \left(\frac{c - c_0}{c_0} \right)^2 + \frac{A_2(c)}{2} |\mathbf{P}|^2 + \frac{A_4}{4} |\mathbf{P}|^4 \right\}, \quad (1)$$

where c_0 is the average density of the suspension, the three terms proportional to B_1, B_2, B_3 couple concentration and splay and are present in equilibrium, C is a compressional modulus and K_1, K_3 are the splay and bending elastic constants. Hereafter we will assume for simplicity $B_1 = B_2 = B_3 \equiv B$ and $K_1 = K_3 = K$. The validity of this assumptions is discussed elsewhere [1,15]; however, they do not qualitatively change the results obtained here. The dynamics of the concentration and the polarization are described by [22]

$$D_t P_i + \omega_{ij} P_j = -\beta_p c \mathbf{P} \cdot \nabla P_i + \lambda u_{ij} P_j + \Gamma h_i - \Gamma' f_i, \quad (2)$$

$$D_t c = -\nabla \cdot \left[\beta_c c^2 \mathbf{P} - \Gamma' h_i - \Gamma'' f_i \right], \quad (3)$$

where $D_t \equiv \partial_t + \mathbf{u} \cdot \nabla$, $h_i = \delta F / \delta P_i$ is the molecular field, $f_i = \partial_i (\delta F / \delta c)$, $u_{ij} = (\partial_i u_j + \partial_j u_i)/2$, $\omega_{ij} = (\partial_i u_j - \partial_j u_i)/2$. Here $\Gamma, \Gamma', \Gamma''$ are kinetic coefficients and β_p, β_c are parameters that arise from self-propulsion, λ is an alignment parameter.

The stress tensor is given by dissipative, reversible, and active contributions:

$$\sigma_{ij}^{\beta} = \frac{\beta_{\sigma}c^2}{\Gamma}[\partial_i P_j + \partial_j P_i + \delta_{ij}\nabla\cdot\boldsymbol{P}], \qquad (4)$$

$$\sigma_{ij}^{\alpha} = \frac{\alpha c^2}{\Gamma}[P_i P_j + \delta_{ij}\Pi], \qquad (5)$$

$$\sigma_{ij}^{r} = -\delta_{ij}\Pi + \frac{\lambda}{2}(P_i h_j + P_j h_i) + \frac{1}{2}(P_i h_j - P_j h_i), \quad (6)$$

where Π is the hydrodynamic pressure. The length and time scales are those typical of low Reynolds numbers ($\ell \sim 1\,\mu$m, $v_0 \sim 10\,\mu$m $\Rightarrow$ $Re \sim 10^{-5}$), hence momentum conservation is provided by the Stokes ($Re = 0$) limit of incompressible fluid flow:

$$\partial_i(\sigma_{ij}^{r} + \sigma_{ij}^{a} + \sigma_{ij}^{\beta} + 2\eta u_{ij}) = 0, \quad \nabla\cdot\mathbf{u} = 0. \qquad (7)$$

The parameters are system and model specific. In particular, the coefficients $\beta_p, \beta_c, \beta_\sigma$ are non-universal phenomenological parameters that depend on the self-propulsion speed v_0 and are determined by microscopic properties. The terms proportional to these coefficients in (2), (3) are exclusive to polar systems. Since they all come from self-propulsion, they can be expressed (using the lengthscales of the system) as: $\beta_p = \beta\ell^2, -\beta_c = \beta'\ell^2, \beta_\sigma = \beta''c_0^2$, where the β, β', β'' have dimensions of velocity and have been estimated in a variety of microscopic models as $\beta_i \sim v_0$ [23–25]. Hereafter, we assume that $\beta = \beta' = \beta''$.

Focussing on the hydrodynamic modes [1], we consider only the orientation of $\mathbf{P}$, expressing it in terms of the polarization angle θ: $\mathbf{P}/|\mathbf{P}| \equiv \mathbf{p} = (\cos\theta, \sin\theta, 0)$. Translational invariance in x, y allows us to reduce the dimension of the problem by assuming $\nabla = (0, \partial_z, 0)$, with all quantities varying in the direction of the film thickness, z only.

We impose a stress-free boundary condition at the surfaces, i.e., $\sigma_{ij}(0, t) = \sigma_{ij}(L, t) = 0$. Stokes equation then implies that $\sigma_{ij}(z, t) = 0$ throughout the film. The incompressibility condition implies $u_z = 0$. On account of Galileian invariance, u_x is determined only up to a constant. For the polarization, we consider BCs with $\mathbf{p}$ parallel to the 2 boundary surfaces, i.e., we consider $\theta(0, t) = \theta(L, t) = 0$ or π. We non-dimensionalise by measuring lengths in units of ℓ, temporal variables in terms of the time scale of splay and bending fluctuations $\tau = \ell^2/K$. A mass scale is set by $\ell^3\tau/\Gamma_0$. The concentration is normalized by the mean density c_0, all the other quantities are redefined accordingly: $z \to z/\ell$, $t \to t/\tau_0 = (K/\ell^2)t$, $\phi(\mathbf{r}, t) \to c(\mathbf{r}, t)/c_0$. Direct substitution in (2), (3) and (7) leads to equations for the dynamics of $\phi(z, t)$ and $\theta(z, t)$ [20].

It is known from linear stability analysis that for $\alpha > \alpha_c$ there is an instability from a quiescent ($\mathbf{u} = \mathbf{0}$) aligned ($\theta = 0$ or π) state to a spontaneous flowing state, with both inhomogeneous alignment and velocity profiles [17,19–22]. The location of the critical value of activity, $\alpha_c(L, \beta)$ depends on BCs. For non-zero $\beta > \beta_c$,

spontaneous oscillations due to the coupling of gradients of concentration to the polarization director appear. Upon increasing β the oscillatory behaviour becomes increasingly complex. Here we restrict ourselves to $\beta < \beta_c$.

Weakly nonlinear analysis: first-order modes. – We can expand the fields about the quiescent state: $\phi(z, t) = \phi_0 + \delta\phi(z, t)$, $\theta(z, t) = \theta_0 + \delta\theta(z, t)$. The BCs imply the following mode expansion:

$$\delta\theta = \sum_{k=1}^{\infty}\Theta_k(t)\sin(k\pi z\ell/L),$$

$$\delta\phi = \sum_{k=1}^{\infty}\Phi_k(t)\cos(k\pi z\ell/L).$$

To get the linear stability threshold we use $\Theta_k(t) = \tilde{\Theta}_k e^{i\omega_k t}, \Phi_k(t) = \tilde{\Phi}_k e^{i\omega_k t}$, with $\tilde{\Theta}_k, \tilde{\Phi}_k$ constant, which substituted into the system of PDEs and keeping terms to linear order, gives a dispersion relation $\omega_k = \omega(k)$, with a steady-state instability (at zero frequency) at a critical value [20]: $\alpha_c(k) = \left(\frac{k\pi\ell}{\phi_0 L}\right)^2\frac{\eta(w-1)}{\lambda-1} + \frac{w\beta[\eta+\frac{1}{2}(1-\lambda)^2]}{(1-\lambda)(D-w)}$, fixing the threshold of linear stability to be $\alpha_c(1)$ of the most unstable mode ($k = 1$).

To test the nonlinear theory to be developed below, we solve the full nonlinear equations numerically. Beyond the onset, the steady-state velocity and density profiles grow in amplitude as the parameters α and β are increased. To resolve the nonlinear dynamics beyond the onset, we use a finite-difference scheme, second order in space and time. The diffusive terms in (3)–(7) are treated implicitly, the other terms explicitly; we implement an adaptive time stepping strategy. The BCs require careful attention, because (3) is conservative and non-constant effective diffusion coefficients appear in it. The dynamics of the profile as it approaches the steady state are shown in the inset of fig. 3, and the stationary profiles obtained are reported in fig. 3, 4. These results show the symmetry breaking noted in the introduction and represented in fig. 1. Indeed, as we can see in fig. 3, 4, the orientation and density profiles present an evident up-down asymmetry with respect to z.

In order to describe the instability theoretically, a first extension of the linear stability result can be obtained by keeping the modes as general functions of t, but restricting the expansion to the 1st mode:

$$\phi(z, t) = \phi_0 + \Phi_1(t)\cos(\pi z\ell/L), \qquad (8)$$
$$\theta(z, t) = \theta_0 + \Theta_1(t)\sin(\pi z\ell/L). \qquad (9)$$

The orthogonality of the trigonometric functions leads to a system of nonlinear first-order ODEs for Θ_1, Φ_1:

$$\dot{\Theta}_1 = f(\Theta_1, \Phi_1) \qquad (10)$$
$$\dot{\Phi}_1 = g(\Theta_1, \Phi_1), \qquad (11)$$

where f, g depend on the parameters of the problem $(D, w, \beta, \alpha, \lambda, \phi_0, \ell/L)$. The system evolves to a steady
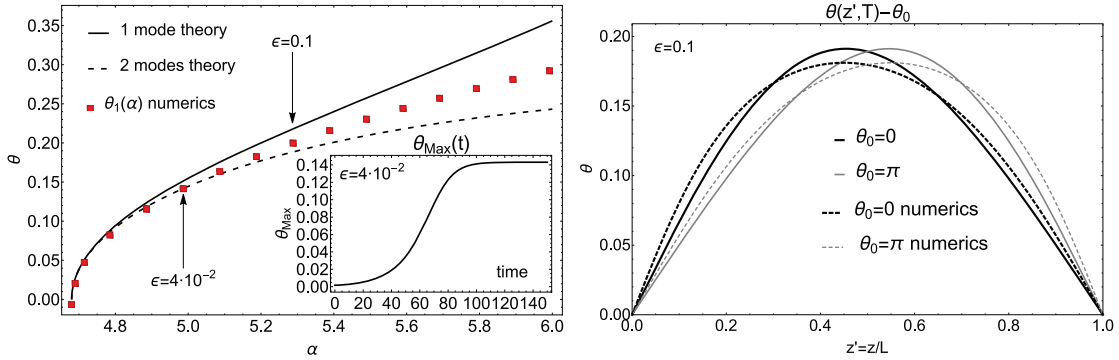
Fig. 3: (Colour online) Left: amplitude of θ as a function of the control parameter α. Numerical simulations (red squares) and theory. The solid line corresponds to the expression $\Theta_1^\star \simeq 0.269(\alpha - \alpha_c)^{1/2}$, whereas the dashed one takes into account the effect of the second mode Θ_2 discussed in the third section. Inset: time dependence of the maximum value of the orientation field throughout the film. Right: stationary profile of orientation across the channel with different BCs, for $\epsilon = 0.1$. Theory (with two modes): $\theta(0,t) = \theta(L,t) = 0$ (black solid line), π (grey solid line), and numerics (black and grey dashed lines). $w = 0.13, \lambda = \beta = 0.1, L = D = 1, \xi = 0, \eta = 0.5$.
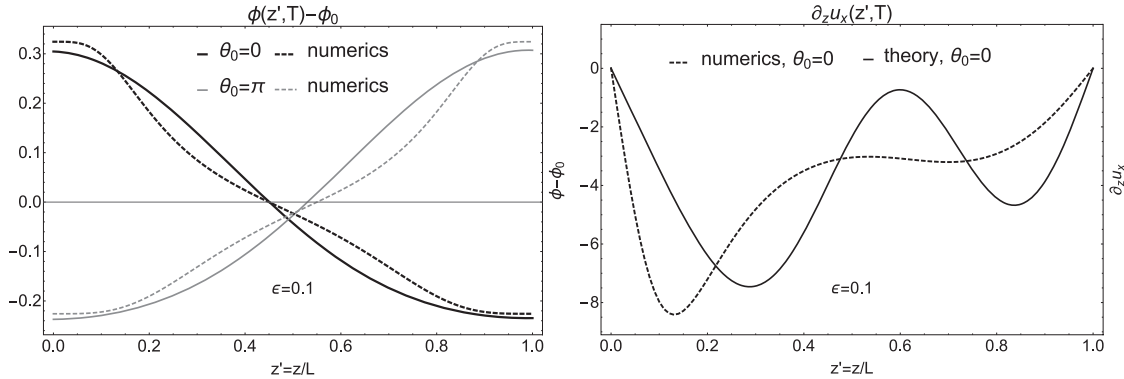
Fig. 4: Left: stationary profile of density across the channel with different BCs, for $\epsilon = 0.1$. Right: velocity gradient profile for $\epsilon = 0.1$, comparison between numerics and theory (with two modes), and $\theta_0 = 0$; the curves for $\theta_0 = \pi$ can be derived by symmetry with respect to the center of the channel. The theory captures the qualitative features of the numerical solution: the presence of two relative minima, and the side of the global one.

state corresponding to a stable non-zero fixed point (Θ_1^*, Φ_1^*), in agreement with numerics, for $\alpha > \alpha_c$. We can identify a control parameter $\epsilon \equiv (\alpha - \alpha_c)/\alpha_c$ and we find fixed point values $\Phi_1^*, \Theta_1^* \sim \epsilon^{1/2}$. A comparison of the analytical solution for $\Theta_1^*(\alpha)$ and the numerically obtained steady-state amplitudes is shown in fig. 3. The results show that very close to the threshold the amplitudes of the stationary profiles are well described by a weakly (first-order) nonlinear theory. However, the first unstable mode for θ is symmetric, and cannot produce the asymmetry observed in the channel (cf. fig. 1), nor the flip caused by the inversion at the boundaries. Consequently, we have to include the terms with $k \geq 2$ appearing in the mode expansion.

Higher-order analysis and instability mechanism: beyond the weakly nonlinear theory. – A generalization of the weakly nonlinear analysis is the theory of amplitude equations [26] which allows one to study the nonlinear stability problem by reorganizing the expansion in the higher modes using the *small* control parameter ϵ, so that the amplitudes of the higher modes decrease with ϵ. This suggests that we can express asymptotically $\Theta_k(t) = \epsilon^{\lambda_k} \theta_k(t)$, where $\lambda_k > \lambda_{k-1}$. The exponents λ_k characterize the decay of the k-wavelength mode in terms of the normalized distance ϵ from the onset of instability, and they are closely connected to the dispersion relation of the system. The exponents λ_k are such that modes with increasing k come into play at increasingly higher orders in ϵ. We can thus for small enough ϵ approximate the solution by truncating the series at $k = N$, to obtain a system of $2N$ ODEs for $\theta_1(t), \phi_1(t), \ldots, \phi_N(t), \theta_N(t)$. To capture the asymmetry in the film, we need to have at least $N = 2$, for which we start by assuming that $\lambda_1 = 1$, $\lambda_2 = 4$: this allows us to keep the contribution of θ_1, ϕ_1 as the dominant one up to the order ϵ^4, at which point θ_2, ϕ_2 appear; the assumption we check to be consistent *a posteriori*. We thus obtain equations
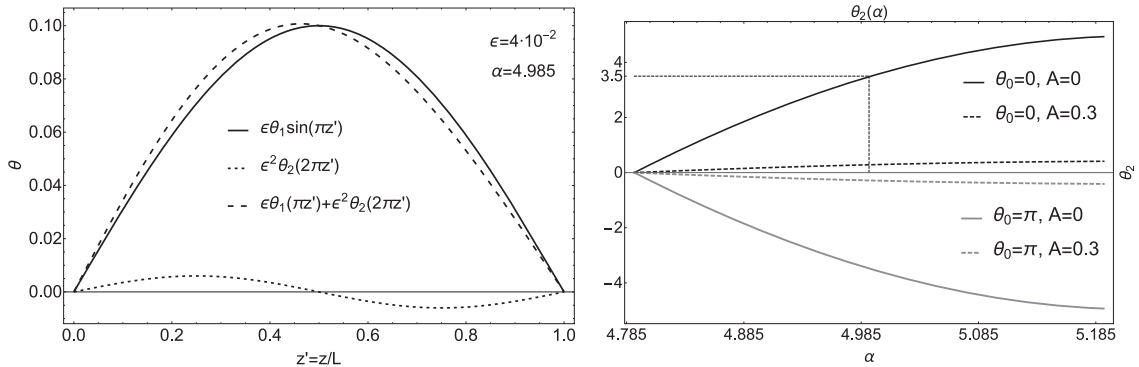
Fig. 5: Left: theoretical profile of θ: the contribution of the second mode gives rise to the asymmetry in the orientation profile $\theta(z, \infty)$. Right: amplitude of the second mode $\theta_2(\alpha)$ as a function of the activity $\alpha > \alpha_c$. The four profiles show θ_2 for two opposite BCs and with the crowding effects discussed in the section "High-densities corrections".

for θ_1, θ_2:

$$\frac{d\theta_1}{dt} = (a_1\theta_1 + b_1\phi_1)\epsilon$$
$$+ (a_3\theta_1^3 + b_3\phi_1^3 + c_{12}\phi_1\theta_1^2 + c_{21}\phi_1^2\theta_1)\epsilon^3, \quad (12)$$

$$\frac{d\theta_2}{dt} = (c_{11}\theta_1\phi_1 + a_2\theta_1^2)\epsilon^2$$
$$+ (d_1\theta_2 + e_1\phi_2 + c_{13}\phi_1^3\theta_1 + c_{31}\phi_1\theta_1^3)\epsilon^4, \quad (13)$$

and similar equations for ϕ_1, ϕ_2. The constant coefficients a_i, c_{ij}, d_i, e_i, ... are reported in the appendix.

The complete set of equations thus found can be solved numerically with $\theta_0 = 0$ and $\theta_0 = \pi$, and we find that a flip in the BCs $\theta(0, t)$, $\theta(L, t)$, reflects into a flip in the amplitude θ_2 of the second mode, as plotted in fig. 5(b) as function of α. This result identifies the origin of the symmetry breaking, that indeed appears as a nonlinear effect due to the higher wavelength modes of the orientation field.

Symmetry breaking can be understood physically in terms of the relationship between the orientation **P** and the density gradient ∇c. The terms with coefficients B_i in the non-equilibrium free energy in (1) are responsible for this coupling, since they give density contributions to the spontaneous splay. They are allowed in equilibrium systems with polar symmetry [25] and model the tendency of **P** to align to the gradients of c, so that splay of one sign enhances and of the other sign reduces the local order expressed by c. Therefore, active particles will tend to have greater orientation variations where the density gradients are higher. Another contribution to this coupling is given by the terms in β that represent the advection of density in (3). In our system, an inversion of the BCs on θ (or, equivalently, **P**) causes a sign change in these terms, which appear in (3) and then cause the final density profile to have a maximum on the opposite side of the channel.

Then, the initial condition (and in particular, its symmetry) selects the shape of the density profile in the stationary state; the zone with highest gradient appears to be on one side of the channel, and on that side the splay

causes a maximum in the variation of θ. When we invert the BCs, *i.e.*, impose $\theta(0, t) = \theta(L, t) = \pi$, the coupling of θ and $\nabla\phi$ acts on the bulk through the nonlinear coupling terms (proportional to B, β), and therefore also the density profile is flipped. Thus, the zone with highest gradients of ϕ and maximum θ is found on the other side of the channel. In agreement with this picture, the asymmetry is seen to increase with α, B or β.

High-density corrections. – Commonly, experiments on active liquid crystals all show a crowded population of self-propelled particles. Being able to adapt the models to high values of $c(\mathbf{r}, t)$ is therefore of great importance to describe real polar suspensions operatively; see also recent experiments [27]. The *crowding effect* can be introduced as a correction to the kinetic parameters in the problem. Whenever a high number of active rods is present in a certain region, *i.e.*, where $c(\mathbf{r}, t)$ is big, their overall speed decreases. This can be modelled by assuming that

$$\Gamma^i(\mathbf{r}, t) = \Gamma_0^i e^{-A\ c(\mathbf{r}, t)/c_0}, \quad (14)$$
$$\eta(\mathbf{r}, t) = \eta_0 e^{A\ c(\mathbf{r}, t)/c_0}, \quad (15)$$

and similarly for β. The effect of this modification is a penalization of the motion of particles in a crowded area of the film. As a result, it smoothes the profile and reduces the asymmetry, as confirmed by our numerical tests. As a result, the amplitude $\theta_2(\alpha)$ has a much smaller value in the case of crowding, causing a less noticeable asymmetry in the solution (see fig. 5(b)).

Discussion. – In conclusion, we showed that active polar films not only show a transition to spontaneous flow above a critical intensity of activity, but they also display a spontaneous symmetry breaking with respect to the transversal direction z. The asymmetry can be inverted when the orientation of the suspension is flipped at the boundaries in the x-direction. This is a typical example of the coupling between density gradients and orientation of polar active particles, that can lead to nonlinear effects,

such as the observed mixing between transversal and parallel modes in the flow in a channel. Moreover, the *crowding* correction devised to account for high densities has the effect of slowing down the instability and smoothing out the density and orientation profiles. From a theoretical perspective, this peculiar nonlinear behaviour offers a wide range of possible directions for further investigation. Along the lines of [28], for instance, it would be of great interest to explore the same system in a more complicated geometry: with a no-slip substrate but surface tension and curvature effects at the top boundary.

Finally, in view of the recent and current progress in the fabrication of active colloids, we expect that symmetry-breaking and other analogous nonlinear phenomena characteristic of polar suspensions can be reproduced and used as a means of transferring input from the parallel to transversal direction of a channel and *vice versa*. This could be of interest in the realization of experiments where operating along one direction proves much harder than acting on the other one.

$$* * *$$

Appendix A: coefficients of the amplitude equations. – The coefficients appearing in (12), (13) are: $a_1 = 4\beta\eta\Gamma_0\phi_0^2/\Omega$, $a_3 = 2\phi_0^2[24(\lambda^2\beta - \alpha) - 1]/9\Omega$, $b_1 = -4\eta\Gamma_0(D - w)$, $b_3 = 0$, $c_{12} = 4\eta\Gamma_0\beta/(3\Omega)$, $c_{21} = 8[(\eta\Gamma_0 + 2\lambda^2)(D - w) + w(1 - \lambda)]/3$, $a_1' = 4[\eta_0\Omega(1 - w) - \phi_0^2(1 - \lambda)/\Omega\alpha]$, $a_3' = 4\Omega[3\eta_0 w + 4\lambda^2(1 - w) - 4\phi_0^2(4\lambda - 1)/(3\Omega^2)\alpha]/3$, $b_1' = 2w[2\eta_0 + (1 - \lambda)^2]$, $c_{21}' = 2[2\eta_0(\beta - w) - (\lambda^2 - 10\lambda + 1)w + 4\phi_0 c_0\beta(1 - \lambda)]/3$, $c_{12}' = -4\alpha(1 - \lambda)\epsilon^3\theta_1\phi_1^2/(3\Omega)$, where $\Omega = \pi\ell/L$. It can be readily noticed that eqs. (12), (13) fall back onto the linear stability result [20], if only the first order in ϵ is considered.

An approximated solution of (12) and (13) can be found by fitting the numerical results, and noticing that for small ϵ the amplitude Θ_1 is well desc with an expression of the form: $\Theta_1 = \Theta_1^\star(\alpha - \alpha_c)^{1/2} \equiv \Theta_1^\star\alpha_c\epsilon^{1/2}$. The same is true for $\Phi_1(\alpha)$, and the numerical prefactors are given in fig. 3. The coefficients for the second mode, are: $D_1 = 24\eta[-\alpha\lambda + \alpha + 4\pi^2\eta(w-1)]$, $D_1' = 12\beta\eta$, $E_1 = 24\pi\eta(D-w)$, $E_1' = \pi[2\eta - (\lambda - 1)^2]w$.

REFERENCES

[1] MARCHETTI M., JOANNY J., RAMASWAMY S., LIVERPOOL T., PROST J., RAO M. and SIMHA R. A., *Rev. Mod. Phys.*, **85** (2013) 1143.

[2] DOMBROWSKI C., CISNEROS L., CHATKAEW S., GOLDSTEIN R. E. and KESSLER J. O., *Phys. Rev. Lett.*, **93** (2004) 098103.

[3] LAUGA E. and POWERS T. R., *Rep. Prog. Phys.*, **72** (2009) 096601.

[4] ZHANG H. P., BE'ER A., SMITH R. S., FLORIN E.-L. and SWINNEY H. L., *EPL*, **87** (2009) 48011.

[5] CHEN X., DONG X., BEER A., SWINNEY H. L. and ZHANG H. P., *Phys. Rev. Lett.*, **108** (2012) 148101.

[6] NÉDÉLEC F., SURREY T. and KARSENTI E., *Curr. Opin. Cell Biol.*, **15** (2003) 118.

[7] KRUSE K., JOANNY F., JÜLICHER F., PROST J. and SEKIMOTO K., *Eur. Phys. J. E*, **16** (2006) 5.

[8] HOWARD J., *Mechanics of Motor Proteins and the Cytoskeleton* (Palgrave Macmillan, Sunderland) 2001.

[9] SCHALLER V., WEBER C., SEMMRICH C., FREY E. and BAUSCH A. R., *Nature*, **467** (2010) 73.

[10] SANCHEZ T., CHEN D. T. N., DECAMP S. J., HEYMANN M. and DOGIC Z., *Nature*, **491** (2012) 431.

[11] GÖTZE I. O. and GOMPPER G., *EPL*, **92** (2010) 64003.

[12] ENCULESCU M. and STARK H., *Phys. Rev. Lett.*, **107** (2011) 058301.

[13] BLAIR D. L., NEICU T. and KUDROLLI A., *Phys. Rev. E*, **67** (2003) 031303.

[14] NARAYAN V., RAMASWAMY S. and MENON N., *Science*, **317** (2007) 105.

[15] DE GENNES P. and PROST J., *The Physics of Liquid Crystals* (Clarendon Press, Oxford) 1993.

[16] SIMHA R. A. and RAMASWAMY S., *Phys. Rev. Lett.*, **89** (2002) 058101.

[17] VOITURIEZ R., JOANNY J. F. and PROST J., *Europhys. Lett.*, **70** (2005) 404.

[18] SAINTILLAN D. and SHELLEY M. J., *Phys. Fluids*, **20** (2008) 123304.

[19] MARENDUZZO D., ORLANDINI E., CATES M. E. and YEOMANS J. M., *Phys. Rev. E*, **76** (2007) 031921.

[20] GIOMI L., MARCHETTI M. C. and LIVERPOOL T. B., *Phys. Rev. Lett.*, **101** (2008) 198101.

[21] MARENDUZZO D., ORLANDINI E., CATES M. and YEOMANS J., *J. Non-Newtonian Fluid Mech.*, **149** (2008) 56.

[22] GIOMI L., LIVERPOOL T. B. and MARCHETTI M. C., *Phys. Rev. E*, **81** (2010) 051908.

[23] LIVERPOOL T. B. and MARCHETTI M. C., *Europhys. Lett.*, **69** (2005) 846.

[24] AHMADI A., LIVERPOOL T. B. and MARCHETTI M. C., *Phys. Rev. E*, **72** (2005) 060901.

[25] KUNG W., MARCHETTI M. C. and SAUNDERS K., *Phys. Rev. E*, **73** (2006) 031708.

[26] CROSS M. and GREENSIDE H., *Pattern Formation and Dynamics in Nonequilibrium Systems* (Cambridge University Press) 2009.

[27] WIOLAND H., WOODHOUSE F. G., DUNKEL J., KESSLER J. O. and GOLDSTEIN R. E., *Phys. Rev. Lett.*, **110** (2013) 268102.

[28] SANKARARAMAN S. and RAMASWAMY S., *Phys. Rev. Lett.*, **102** (2009) 118107_1.